Nanoscale

COMMUNICATION

View Article Online
View Journal

Check for updates

Cite this: DOI: 10.1039/c7nr03895j

Received 2nd June 2017,
Accepted 30th July 2017

DOI: 10.1039/c7nr03895j

rsc.li/nanoscale

Published on 01 August 2017. Downloaded by Zhejiang University on 22/08/2017 02:12:57.

# Dry spinning approach to continuous graphene fibers with high toughness†

Qishi Tian,[a] Zhen Xu,*[a] Yingjun Liu,[a] Bo Fang,[a] Li Peng,[a] Jiabin Xi,[a] Zheng Li[a] and Chao Gao*[a,b,c]

**Graphene fiber (GF) has emerged as a new carbonaceous fiber species since graphene-based liquid crystals were discovered. The growing performances of GFs in terms of their mechanical performance and their functionalities have assured their extensive applications in structural materials and functional textiles. To date, many spinning strategies utilizing coagulation baths have been applied in GF, which necessitates a complicated washing process. Dry spinning is a more convenient and green method for use with fibers in the chemical fiber industry, and should be a good option for GFs; however, this technique has never been used in a system of GF. In this research, first the dry spinning technique was used to fabricate continuous GFs and the dry spun GFs showed good toughness and flexibility. The dry spinnability of graphene oxide liquid crystals was achieved by choosing dispersive solvents with low surface tension and high volatility. The dry spun neat GFs possessed high toughness up to 19.12 MJ $m^{-3}$, outperforming the wet spun neat GFs. This dry spinning methodology facilitates the green fabrication of fibers of graphene and graphene-beyond two-dimensional nanomaterials, and it may also be extended to other printing technologies for complex graphene architectures.**

## Introduction

Graphene with its outstanding electrical, mechanical and thermal properties has attracted considerable interest for fabricating advanced macroscopic carbonaceous materials using bottom-up assembly.[1–4] Macroscopic one-dimensional (1D) fibers have recently emerged as a very interesting species of graphene macroscopic materials.[5–8] Because of the intriguing properties of the constituent graphene, graphene fibers (GFs) have exhibited great potential as high performance and multifunctional lightweight carbonaceous fibers. For their production, six methods have been developed, including wet spinning,[5–7,9] electrospinning,[10] hydrothermal,[11,14,18] electrophoretic assembly,[13] dry jet wet spinning[14,22] and film conversion.[15–17,39,40] Among these, a wet spinning strategy based on the liquid crystals (LCs) of a solvated graphene precursor is the one most likely to be applied when the method is moved from laboratory scale to industry scale in the future. However, this method still needs coagulating baths, which makes the process complicated and increases the production costs.

Dry spinning is a more convenient and green method, and has been applied in the chemical fiber industry. Because of its slow fiber forming process, the polymer fibers are uniform and dense.[35] Therefore, the dry spinning strategy may be favored because of the compactness and uniformity of the graphene oxide (GO) fiber, which may contribute to the enhancement of the electrical conductivity, and the mechanical and thermal properties. Meanwhile, it does not require a coagulating bath, which simplifies the fiber spinning process and decreases the production cost. However, the dry spinning of GFs has never been realized, possibly because of high surface tension and low saturated vapor pressure of the GO spinning dopes [*e.g.*, water ($H_2O$) and *N*,*N*-dimethylformamide (DMF)] which limit the spinnability. These solvents with high surface tension aggravate the tendency of GO dopes to shrink to droplets and their low saturated vapor pressure slows down the rate of solidification to form dry fibers, which makes the GO aqueous dispersion and the DMF dispersion failed to fabricate continuous GFs *via* a dry spinning strategy. Thus, in order to realize the dry spinning of GF, the dispersibility, the surface tension and volatility of the solvents of the spinning dopes should be properly balanced.

In this research, methanol, ethanol, acetone and tetrahydrofuran (THF) with water were chosen as the mixed

[a]*MOE Key Laboratory of Macromolecular Synthesis and Functionalization, Department of Polymer Science and Engineering, Zhejiang University, 38 Zheda Road, Hangzhou 310027, PR China. E-mail: zhenxu@zju.edu.cn, chaogao@zju.edu.cn*

[b]*Key Laboratory of Adsorption and Separation Materials & Technologies of Zhejiang Province, Zhejiang University, 38 Zheda Road, Hangzhou 310027, PR China*

[c]*State Key Laboratory for Modification of Chemical Fibers and Polymer Materials, Donghua University, Shanghai 201620, PR China*

†Electronic supplementary information (ESI) available: Materials and characterization for the experiment. Twelve figures and two tables. See DOI: 10.1039/c7nr03895j

Published on 01 August 2017. Downloaded by Zhejiang University on 22/08/2017 02:12:57.

solvents of GO for dry spinning. Once the solvents were chosen, a simple dry spinning was developed and continuous GFs were fabricated without using any coagulating baths. The dry spun GF reached a comparable level in mechanical strength (up to 375 MPa) to wet spun GFs, but had a better toughness, up to 19.12 MJ $m^{-3}$, than their wet spun counterparts. The dry spinning strategy for GFs is convenient, energy saving and environmentally friendly. It may also be possible to extend it to the macroscopic assembly of other nanomaterials and printing technologies for complex graphene architectures.

## Results and discussion

A GO aqueous dispersion was prepared from graphite using a modified Hummers' method, which was described in previous papers.[38] GO sheets have an average size of 52 μm with a wide distribution ranging from 5 μm to 150 μm (Fig. S1, ESI†). Previously, GFs have been fabricated continuously from the GO aqueous dispersion and DMF dispersions using a wet spinning method.[5,6]

In the beginning, the dry spinning was tried by extruding the GO aqueous dispersion and neat DMF dopes directly into the air, and these two dopes with a high surface tension and low volatility were found to be not suitable for the dry spinning (Fig. 1). Then the effect of GO concentration on the spinnability was investigated. When the concentration was low (about 4.5 mg $g^{-1}$), the droplet formed on the syringe nozzle. This was because the gel dispersion in the nozzle cannot maintain its original fibrous shape when the GO dopes left the nozzle, which can be proved by the low storage modulus of GO aqueous dispersion.[21] At a high concentration up to 14 mg $g^{-1}$, although the fiber can maintain its original shape when being extruded, it was also prone to form a droplet at the end of the gel fiber because of the high surface tension of the $H_2O$ and DMF (Table S1, ESI†) and hard to collect continuously because of the low drying rate.

### Criteria for dry spinning of continuous graphene fibers

According to the 1D hydrodynamics model, a fluid stream shows the Rayleigh instability which has a close relationship with the surface tension of the fluid.[32] The low surface tension decreased the tendency of the GO dispersion to shrink to a droplet, which would be of benefit for the stability of the gel fibers when the GO dopes left the nozzle (Fig. 1b). A low boiling point together with the high saturated vapor pressure of the solvents contributes to the fast drying of GO gel fiber, which is favorable for the collection of continuous GFs. Therefore, to achieve the dry spinning of continuous GFs, the

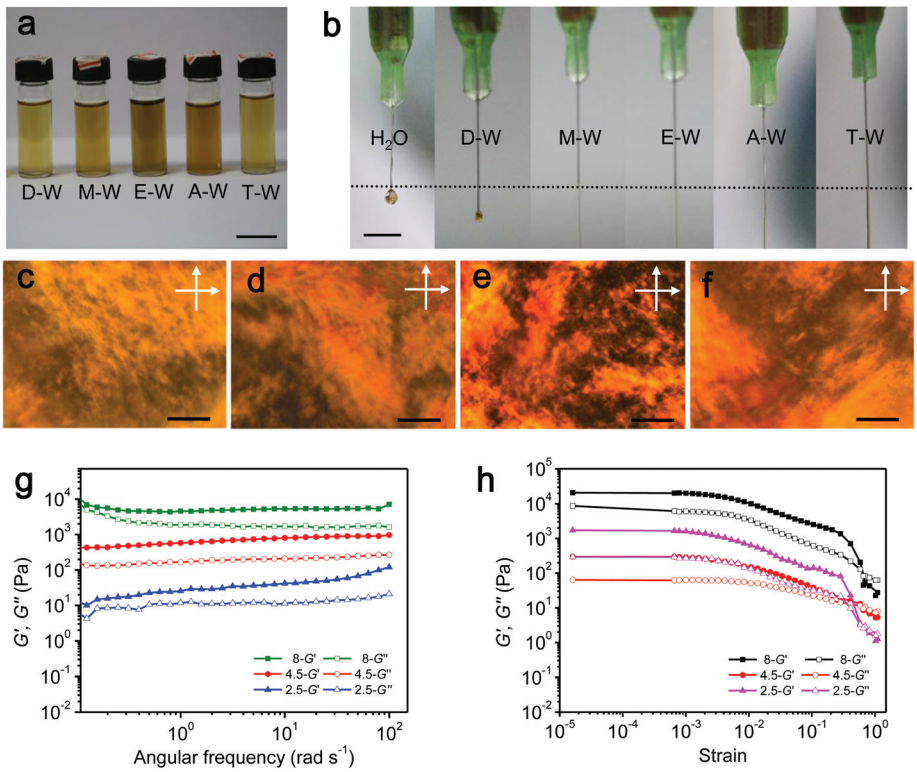


**Fig. 1** Spinnability of GO dispersions with different solvents. (a) 1 mg $g^{-1}$ GO dispersion with different solvents including DMF–$H_2O$, methanol–$H_2O$, ethanol–$H_2O$, acetone–$H_2O$ and THF–$H_2O$, abbreviated as D–W, M–W, E–W, A–W and T–W, respectively. All the volume ratios were 1 : 1. Scale bar: 1.5 mm. (b) GO gel fiber or droplet with different solvents ($H_2O$, D–W, M–W, E–W, A–W and T–W). Scale bar: 0.6 mm. The POM images of 14 mg $g^{-1}$ GO dispersions with different solvents including methanol–$H_2O$ (c), ethanol–$H_2O$ (d), acetone–$H_2O$ (e) and THF–$H_2O$ (f). Scale bar: 500 μm. (g) and (h) Rheology properties of the GO THF dispersion with different concentrations (2.5 mg $g^{-1}$, 4.5 mg $g^{-1}$, 8 mg $g^{-1}$).

 This journal is © The Royal Society of Chemistry 2017

Published on 01 August 2017. Downloaded by Zhejiang University on 22/08/2017 02:12:57.

dispersibility, the surface tension and volatility of solvents all have to be balanced.

### Dispersibility of GO dry spun dopes

Guided by the criteria for solvents, we examined several other polar solvents with low surface tension, low boiling point, and high saturated vapor pressure to disperse GO homogenously including methanol, ethanol, acetone and THF (Table S1, ESI†). The dispersibility of the GO sheets has a close link with the Hansen solubility parameters of solvents, and this parameter system has three components: polar interaction ($\delta_p$), hydrogen bonding interactions ($\delta_h$), and dispersion forces in solutions ($\delta_d$), as shown in Table S2 (ESI†).[19,21] In view of this, the ratio between water and organic solvents was adjusted to keep the dispersion of the GO sheets homogeneous (Fig. 1a). In these solvents, the observed nematic LCs demonstrated, under a polarized optical microscope (POM), their stable and homogenous dispersive state, as shown by the spreading Schlieren textures (Fig. 1c–f). GO LCs with ordering alignment show promise for assembling macroscopic fibers from individual GO sheets.[5] Thus, these GO dispersions in the chosen solvents with liquid crystalline attributes enable the fabrication of GO fibers with aligned structure using dry spinning.

### Effect of the surface tension and volatility of solvents on the spinnability of GO dopes

The surface tension of the doping solvents together with their volatility plays a vital role in formatting and maintaining continuous fibers from the nozzle to the collecting drum. The volume ratio between the organic solvent and $H_2O$ was adjusted so that the surface tension and volatility of the mixed solvents could be changed to investigate the spinnability of GO dopes. It was found that the higher the content of organic solvent, the easier it was to obtain a continuous GO fiber. In the example of the THF system, when the percentage volume of THF was 25%, the length of the gel fiber collected was only ~5 cm, whereas the gel fiber can be collected continuously when the percentage volume of THF was 50%, which agreed with the effect of surface tension and volatility as stated previously.

### Effect of concentration of GO dopes on the spinnability

The GO/THF–$H_2O$ (volume ratio of THF and $H_2O$ was 1 : 1) dispersion was chosen as an example to systematically investigate the spinnability and the mechanical/electrical properties of the dry spun fibers. When the concentration of the GO dispersion was lower than 4.5 mg $g^{-1}$, the GO THF dispersion did not form a fiber but a droplet, which was similar to the GO neat aqueous dispersion (Fig. S3, ESI†). Further increasing the concentration to 8 mg $g^{-1}$, continuous GO fibers were obtained (Fig. 2). This can be explained by the concentration-dependent rheological behavior of the GO dispersion [Fig. 1g, h and S5 (ESI†)].

At a relatively low concentration of 2.5 mg $g^{-1}$, GO sheets were randomly dispersed in the dispersion with a small zero shear viscosity ($\eta_0$; 10 Pa s) and elastic modulus ($G'$; 10 Pa) [Fig. 1g and S5 (ESI†)]. Upon increasing the concentration to 4.5 mg $g^{-1}$, the GO dispersion possessed a gel-like behavior with a high elastic modulus of 426–969 Pa (Fig. 1g), even higher than that of the GO aqueous dispersion (350–490 Pa) at 13.35 mg $ml^{-1}$.[20] The zero shear viscosity increased as well, with the increasing concentration. GO dispersions above 4.5 mg $g^{-1}$ were viscoelastic LC gels which were suitable for dry spinning. Further increasing the concentration up to 8 mg $g^{-1}$ resulted in a distinct increase of the zero shear viscosity and the moduli ($G'$, $G''$). The $G'$ approached 10 kPa and the $G'/G''$ was close to 10 kPa, indicating that there was a strong interaction among the adjacent GO sheets (Fig. 1g).[34] Because of the high $G'$, the GO gel fiber can maintain its shape and be collected continuously. When the GO organic dispersion was extruded out through a syringe nozzle, the loss modulus ($G''$) became dominant because of shear thinning effect [Fig. 1h

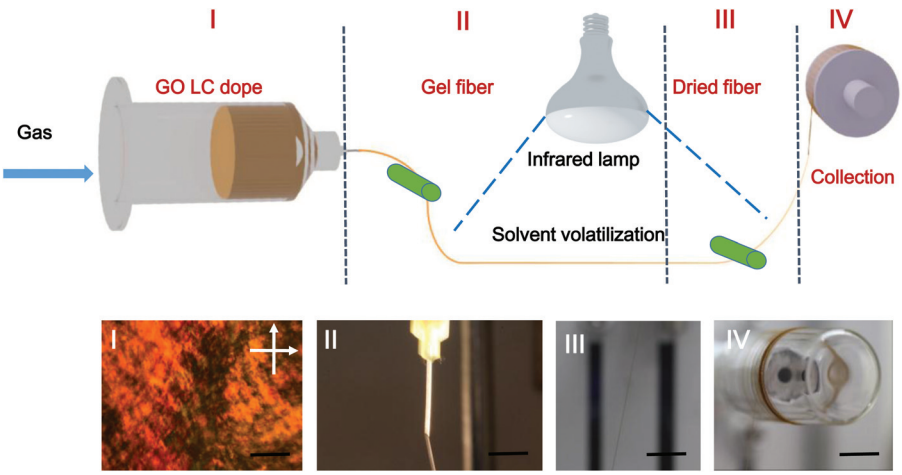


Fig. 2 Schematic illustration of the dry spinning process with a concentrated organic dispersion of GO. (I) POM image of the GO dispersion. Scale bar: 500 μm. (II) Digital photograph of the nozzle with a suspended GO gel fiber. Scale bar: 0.6 mm. (III) Digital photograph of the drying fiber. Scale bar: 2 cm. (IV) Photograph of a GO fiber wound on a glass bottle. Scale bar: 2 cm.

Published on 01 August 2017. Downloaded by Zhejiang University on 22/08/2017 02:12:57.

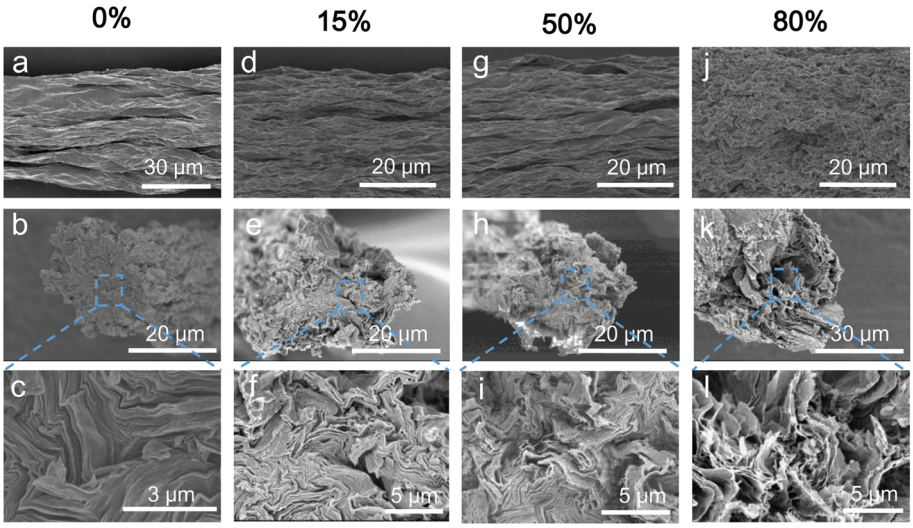


**Fig. 3** SEM images showing the surface morphology and transverse section of the GO fibers. The surface morphology of GO fibers with different shrink ratios including 0% (a), 15% (d), 50% (g) and 80% (j). The transverse section of GO fibers with different shrink ratios including 0% (b), 15% (e), 50% (h) and 80% (k). The magnified images of the top SEM images (c), (f), (i) and (l), respectively.

and S4 (ESI†)]. However, when the liquid crystal GO viscoelastic gels left the needle, the elastic modulus ($G'$) became the dominant factor. The interactions include van der Waals forces and the hydrogen bonds among the GO sheets make the gel fibers regain their high elasticity which maintains its intrinsic fiber shape. The rheology measurements illustrated that the elastic modulus increased as the strain became small (Fig. 1h), which can maintain the fibrous shape of the self-standing GO gel for the continuous fibre collection. The GO fiber can be collected continuously at a rate of 10 mm $s^{-1}$ by controlling the temperature around the fiber with a nozzle (130 μm) [Fig. 2, Movie S1 (ESI†)].

### Controlling the conditions of the spinning process

The homemade dry spinning apparatus consists of an injection pump, an infrared lamp and a rotating drum (Fig. 2). The GO dopes were extruded with a nozzle with a diameter of 130 μm at a rate of 10 mm $s^{-1}$. The temperature around fiber can be up to 80 °C with the help of the infrared lamp so that the solvent in fiber can evaporate and the fiber can be collected continuously. In the process, a significant shrinkage was observed in both the axial and radial direction of the gel fibers. Typically, the axial shrinkage determined the flexibility and toughness of the spun GO and reduced graphene oxide (rGO) fibers, which can be controlled by adjusting the shrinkage ratio. Using POM [Fig. S2, Movie S2 (ESI†)], the liquid crystalline textures of the gel fibers were observed, indicating that the GO sheets maintained a regular arrangement along the gel fiber axial direction. About 90 s later, the solvent in the GO gel fiber volatilized completely, and the diameter of GO fiber shrank to 23 μm, about 1/6 of the original length of the GO gel fiber (130 μm). As the solvents among the GO sheets volatilized from the GO gel fiber, the emerging capillary force leads to the press stress of the GO sheets. This gives rise to the GO sheets contracting inward and crimping along the radial direction of the fiber, causing it to buckle into numerous aligned wrinkles along the axial direction of the fiber (Fig. 3).

### Mechanical properties of GO and rGO fibers

The typical tensile strength–strain curves of GO and rGO fibers are shown in Fig. 4a. The tensile strength of the GO fiber was ~180 ± 30 MPa and the elongation at break was ~4 ± 0.3%. After reduction using hydriodic acid (HI), the tensile strength of the rGO fibers increased to 375 ± 20 MPa, and the elongation at break and electrical conductivity increased up to 9.4% and 1.32 × $10^4$ S $m^{-1}$, respectively. The toughness of the rGO fibers was calculated to be 19.12 ± 2 MJ $m^{-3}$, one order of magnitude greater than that of natural nacre (1.8 MJ $m^{-3}$)[29] and bone (1.2 MJ $m^{-3}$),[30] and better than that previously reported for neat GFs (Fig. 4c and d, Table 1). Additionally, this value surpasses that of graphene/polymer composite fibers such as GO/polypyrrole fiber (0.8 MJ $m^{-3}$),[23] rGO/poly(vinyl alcohol) (PVA) fiber (2.4 MJ $m^{-3}$),[24] GO/nanofibrillated cellulose fiber (4.9 MJ $m^{-3}$),[25] GO/poly(glycidyl methacrylate) fiber (7.8 MJ $m^{-3}$),[26] Go-grafted-poly(acrylonitrile) (GO-*g*-PAN) fiber (12.3 MJ $m^{-3}$)[27] and giant graphite oxide/hyperbranched polyglycerol (GGO/HPG) fiber (18 MJ $m^{-3}$)[28,31] (Fig. 4d). The toughness of the dry spun GF reported in this paper is weaker than that (1380 MJ $m^{-3}$) of a ternary graphene composite fiber (graphene–carbon nanotubes-PVA) in mechanical performance; however, the conductivity is 1.32 × $10^4$ S $m^{-1}$ which is higher than that (0.021 S $m^{-1}$) of the composite fiber, which is significantly useful for multifunctional use as smart textiles.[36,37]

### Mechanism of the flexibility and toughness of dry spun fibers

To explore the origin of the excellent flexibility, the shrinkage ratio of the free standing gel fiber was controlled by adjusting the distance ($L_0$) of two ends of the gel fiber (Fig. S7; ESI†). The

 This journal is © The Royal Society of Chemistry 2017

Published on 01 August 2017. Downloaded by Zhejiang University on 22/08/2017 02:12:57.

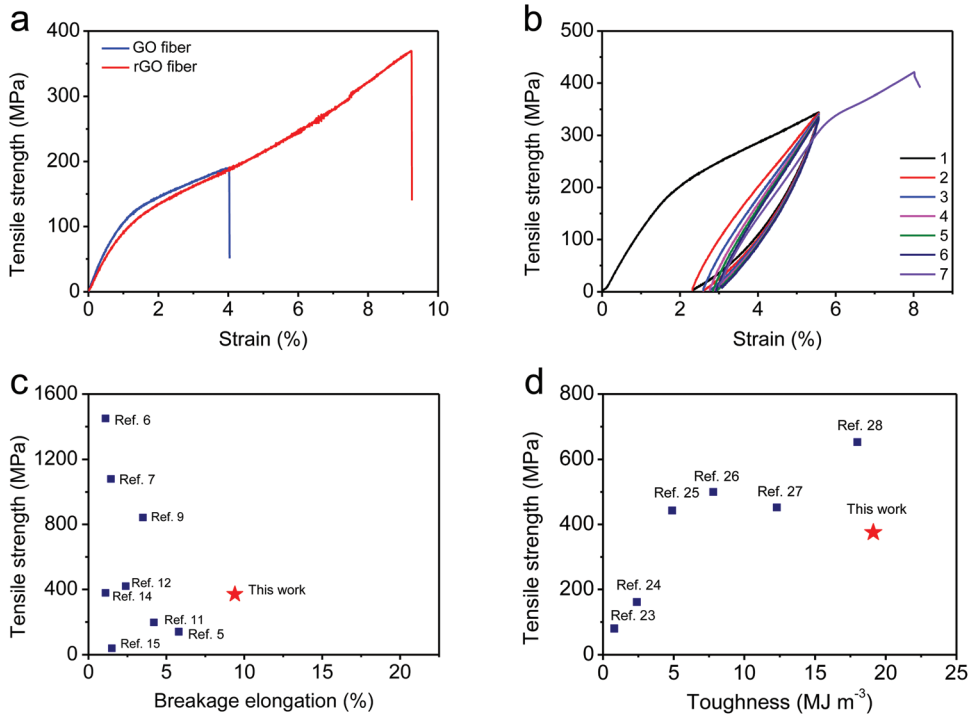


**Fig. 4** Mechanical properties of GO and rGO fibers. (a) Tensile strength–strain curves of GO and rGO fibers. (b) Typical cycle tensile strength–strain curves of rGO fiber. (c) Comparison of tensile strength–breakage elongation between our dry spun GF and reported neat GFs. (d) Comparison of tensile strength–toughness between dry spun neat GF and graphene/polymer composite fiber.

**Table 1** Comparison of the mechanical and electrical properties of rGO fibers in this paper and previous papers

| Tensile strength (MPa) | Breaking elongation (%) | Young's modulus (GPa) | Toughness (MJ $m^{-3}$) | Electrical conductivity ($10^4$ S $m^{-1}$) | Ref. |
|---|---|---|---|---|---|
| 375 | 9.4 | 11.6 | 19.12 | 1.32 | This work |
| 140 | 5.8 | 7.7 | — | 2.5 | 5 |
| 1450 | 1.1 | 282 | — | 80 | 6 |
| 1080 ± 61 | 1.45 | 77.6 ± 8.1 | — | 11.1 ± 0.5 | 7 |
| 842.6 | 3.5 | — | 15.8 | 2.924 | 9 |
| 197 | 4.2 | — | — | 0.12 | 11 |
| 420 | 2.4 | — | — | 0.1 | 12 |
| — | — | — | — | 0.66 | 13 |
| 378 | 1.10 | 36.2 | — | 2.85 | 14 |
| 39.2 | 1.5 | 3.170 | 0.3 | 4.16 | 15 |
| 150 | 20 | 1.9 | — | 0.08 | 18 |

shrinkage ratio ($R$) was defined as the ratio of the reduced length ($L_0$–$L$) to the original length ($L_0$) of the free standing gel fiber, where $L$ was the linear distance of the two supports. In comparison, fibers without shrinkage featured the most uniform orientation of wrinkles along the fiber axis and compact cross-section morphology (Fig. 3a). As the shrinkage ratio increased to 50%, the partial orientation along the axial direction transforms into wrinkles (Fig. 3g), whereas a freely drying fiber with a shrinkage ratio of 80% displayed random wrinkles and porous structure (Fig. 3j). The orientation of wrinkles directly influenced the mechanical properties of the GFs. Uniaxial tension tests revealed the fracture behavior of fibers with different shrinkage ratios from 0% to 80% (Fig. S10b; ESI†). The fiber without shrinkage displayed a small failure strain (3.5%), whereas the fiber with a shrinkage ratio of 80% possessed a large failure strain (35%). For the former, the tensile strength was higher, resulting from more compact stacking among graphene sheets, together with their improved alignment. For the latter, its highly wrinkled structure along the axial direction can maintain a moderate breakage strain, but with a lower strength because of the porous structure.[33] The GO fiber with the shrinkage ratio of 80% possessed the highest toughness up to 10.77 MJ $m^{-3}$ (Fig. S10c; ESI†). In this context, the shrinkage ratio can be balanced and GFs can be designed with high toughness or high strength for various target applications.

Published on 01 August 2017. Downloaded by Zhejiang University on 22/08/2017 02:12:57.

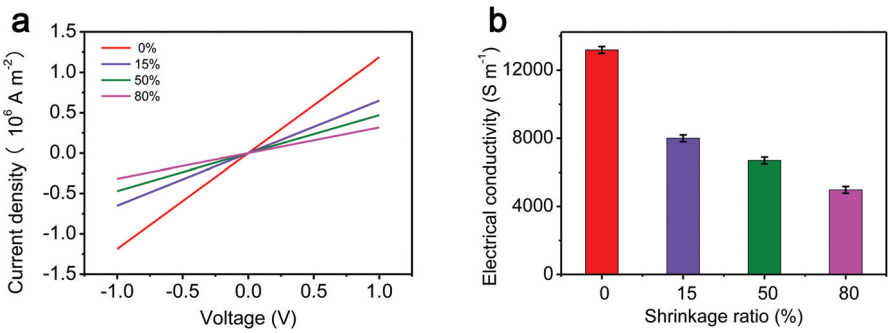


Fig. 5 Electrical properties of rGO fiber with different shrinkage ratio. (a) Current density–voltage curves of rGO fibers. (b) The increasing electrical conductivity of rGO fibers with decreasing shrinkage ratio.

The presence of interlocked wrinkles increases the failure strains of rGO fibers.[34] This conclusion has been confirmed by the cyclic tensile strength–strain measurement of the rGO fiber. As shown in Fig. 4b, cyclic loading–unloading curves within a given strain region between 2.5% and 5% show that a permanent deformation occurs under loading with stretching interlocked wrinkles. The electrical conductivity of rGO fibers with different shrinkage ratios was also investigated (Fig. 5a and b). The fiber without shrinkage possessed the best electrical conductivity ($1.32 \times 10^4$ S m$^{-1}$) and the fiber with the highest shrinkage ratio (80%) had the lowest electrical conductivity ($4.97 \times 10^3$ S m$^{-1}$). The fibers without shrinkage presented an oriented alignment structure with a higher degree of orientation and compactness that benefited the transport of electrons in the fiber. Upon increasing the shrinkage ratio, the fiber presented partial or random wrinkles with a lower degree of orientation and compactness which would restrict the transport of electrons.

### Effect of the volume ratio of THF in the mixed solvents on the mechanical properties of the dry spun fiber

The effect of the content of organic solvent on the mechanical properties of the corresponding fibers was also investigated. It was found that the higher content of organic solvent (THF), the lower the tensile strength of the GO fiber obtained. When the volume percentage of THF was 25%, the tensile strength of the GO fiber was the highest at up to 200 MPa. Nevertheless, when the volume ratio (THF/$H_2O$) was higher than 90%, the tensile strength of fiber decreased quickly (Fig. S10a; ESI†). As the content of THF was increased, more voids in the cross section of GO fiber were observed as shown in Fig. S6 (ESI†), and this was possibly caused by the fast evaporation rate hindering the stacking of the GO sheets.

## Conclusion

The fabrication of continuous GF was realized *via* a convenient dry spinning method. The dry spinning of GF excludes the use of coagulating baths, which simplifies the spinning process when compared with the previous wet spinning method. The dry spinning strategy creates a promising new route for constructing flexible and robust GFs in the future and providing an alternative way for the macroscopic assembly of graphene beyond two-dimensional materials. This method may be extended to other printing technologies for complex graphene architectures.

## Experimental section

### Preparation of spinning dopes

GO aqueous dispersion was prepared using a modified Hummers' method. Briefly, potassium permanganate (60 g) was slowly added into concentrated sulfuric acid (500 ml) in a round bottomed flask under constant stirring at room temperature. Afterwards, natural graphite powder (500 μm, 12 g) was slowly added under constant stirring. The mixture was kept at room temperature for 72 h, and poured into 6 L of cooled deionized water. Then, 25 ml of hydrogen peroxide (30%) was added until the gas was given off completely, and the mixture was washed with an aqueous solution of hydrochloric acid (37%, 100 ml) to remove the manganese ions. Subsequently, the pH of the product was adjusted to neutral with deionized water. The GO dispersion obtained was centrifuged at 2000 rpm for 30 min to remove the small flaked GO. Finally, the GO aqueous dispersion was concentrated to about 14 mg g$^{-1}$ at 8500 rpm for 10 h.

From the GO aqueous dispersions, water was replaced with ethanol and other solvents using repeated centrifugation. GO dispersions with different volume ratios of organic solvents were obtained by controlling the content of the organic solvents.

### Dry spinning of GO fiber

On a homemade dry spinning apparatus, GO organic dopes were extruded through a spinneret with an inner diameter of 130 μm at a rate ranging from 1 to 10 mm s$^{-1}$. When we collected wet fibers and dried them on the surface of drums, ribbons were obtained. Therefore, we used infrared light to heat gel fibers to form dry fibers before collection. The reel together with the fibers was transferred into an oven and dried thoroughly at 60 °C for 12 h.

 This journal is © The Royal Society of Chemistry 2017

Published on 01 August 2017. Downloaded by Zhejiang University on 22/08/2017 02:12:57.

**Reduction of GO fiber**

The GO fibers were reduced using HI : ethanol (1 : 3 volume ratio) for 12 h at 80 °C. After cooling to room temperature, the fibers were washed three times with ethanol. Then, rGO fibers were obtained after drying at ambient environment for 12 h.

## Conflicts of interest

The authors declare no competing financial interest.

## Acknowledgements

This work is supported by the National Natural Science Foundation of China (No. 51533008, 21325417, 51603183), National Key R&D Program of China (Grant No. 2016YFA0200200), Fundamental Research Funds for the Central Universities (No. 2017QNA4036, 2017XZZX008-006), Hundred Talents Program of Zhejiang University (188020*194231701/113), National Postdoctoral Program for Innovative Talents (No. BX201700209) and the State Key Laboratory for Modification of Chemical Fibers and Polymer Materials, Donghua University (No. LK1403).

## References

1 X. Du, I. Skachko, A. Barker and E. Y. Andrei, *Nat. Nanotechnol.*, 2008, **3**, 491.
2 C. Lee, X. Wei, J. W. Kysar and J. Hone, *Science*, 2008, **321**, 385.
3 J. H. Seol, I. Jo, A. L. Moore, L. Lindsay, Z. H. Aitken, M. T. Pettes, X. Li, Z. Yao, R. Huang, D. Broido, N. Mingo, R. S. Ruoff and L. Shi, *Science*, 2010, **328**, 213.
4 K. S. Novoselov, A. K. Geim, S. V. Morozov, D. Jiang, Y. Zhang, S. V. Dubonos, I. V. Grigorieva and A. A. Firsov, *Science*, 2004, **306**, 666.
5 Z. Xu and C. Gao, *Nat. Commun.*, 2011, **2**, 571.
6 Z. Xu, Y. Liu, X. Zhao, L. Peng, H. Sun, Y. Xu, X. Ren, C. Jin, P. Xu, M. Wang and C. Gao, *Adv. Mater.*, 2016, **28**, 6449.
7 G. Xin, T. Yao, H. Sun, S. M. Scott, D. Shao, G. Wang and J. Lian, *Science*, 2015, **349**, 1083.
8 Z. Li, Z. Liu, H. Sun and C. Gao, *Chem. Rev.*, 2015, **115**, 7046.
9 Y. Zhang, Y. Li, P. Ming, Q. Zhang, T. Liu, L. Jiang and Q. Cheng, *Adv. Mater.*, 2016, **28**, 2834.
10 Q. Bao, H. Zhang, J. Yang, S. Wang, D. Y. Tang, R. Jose, S. Ramakrishna, C. T. Lim and K. P. Loh, *Adv. Funct. Mater.*, 2010, **20**, 782.
11 D. Yu, K. Goh, H. Wang, L. Wei, W. Jiang, Q. Zhang, L. Dai and Y. Chen, *Nat. Nanotechnol.*, 2014, **9**, 555.
12 Z. Dong, C. Jiang, H. Cheng, Y. Zhao, G. Shi, L. Jiang and L. Qu, *Adv. Mater.*, 2012, **24**, 1856.
13 E. Y. Jang, J. Carretero-González, A. Choi, W. J. Kim, M. E. Kozlov, T. Kim, T. J. Kang, S. J. Baek, D. W. Kim, Y. W. Park, R. H. Baughman and Y. H. Kim, *Nanotechnology*, 2012, **23**, 235601.
14 C. Xiang, N. Behabtu, Y. Liu, H. G. Chae, C. C. Young, B. Genorio, D. E. Tsentalovich, C. Zhang, D. V. Kosynkin, J. R. Lomeda, C.-C. Hwang, S. Kumar, M. Pasquali and J. M. Tour, *ACS Nano*, 2013, **7**, 1628.
15 R. Cruz-Silva, A. Morelos-Gomez, H.-i. Kim, H.-k. Jang, F. Tristan, S. Vega-Diaz, L. P. Rajukumar, A. L. Elías, N. Perea-Lopez, J. Suhr, M. Endo and M. Terrones, *ACS Nano*, 2014, **8**, 5959.
16 F. Meng, W. Lu, Q. Li, J.-H. Byun, Y. Oh and T.-W. Chou, *Adv. Mater.*, 2015, **27**, 5113.
17 Z. Xu and C. Gao, *Mater. Today*, 2015, **18**, 480.
18 J. Li, J. Li, L. Li, M. Yu, H. Ma and B. Zhang, *J. Mater. Chem. A*, 2014, **2**, 6359.
19 S. Park, J. An, I. Jung, R. D. Piner, S. J. An, X. Li, A. Velamakanni and R. S. Ruoff, *Nano Lett.*, 2009, **9**, 1593.
20 S. Naficy, R. Jalili, S. H. Aboutalebi, R. A. Gorkin III, K. Konstantinov, P. C. Innis, G. M. Spinks, P. Poulin and G. G. Wallace, *Mater. Horiz.*, 2014, **1**, 326.
21 R. Jalili, S. H. Aboutalebi, D. Esrafilzadeh, K. Konstantinov, S. E. Moulton, J. M. Razal and G. G. Wallace, *ACS Nano*, 2013, **7**, 3981.
22 S. Seyedin, M. S. Romano, A. I. Minett and J. M. Razal, *Sci. Rep.*, 2015, **5**, 14946.
23 X. Ding, Y. Zhao, C. Hu, Y. Hu, Z. Dong, N. Chen, Z. Zhang and L. Qu, *J. Mater. Chem. A*, 2014, **2**, 12355.
24 L. Kou and C. Gao, *Nanoscale*, 2013, **5**, 4370.
25 Y. Li, H. Zhu, S. Zhu, J. Wan, Z. Liu, O. Vaaland, S. Lacey, Z. Fang, H. Dai, T. Li and L. Hu, *NPG Asia Mater.*, 2015, **7**, e150.
26 X. Zhao, Z. Xu, B. Zheng and C. Gao, *Sci. Rep.*, 2013, **3**, 3164.
27 Z. Liu, Z. Xu, X. Hu and C. Gao, *Macromolecules*, 2013, **46**, 6931.
28 X. Hu, Z. Xu, Z. Liu and C. Gao, *Sci. Rep.*, 2013, **3**, 2374.
29 R. Z. Wang, Z. Suo, A. G. Evans, N. Yao and I. A. Aksay, *J. Mater. Res.*, 2001, **16**, 2485.
30 J. Y. Rho, L. K. Spearing and P. Zioupos, *Med. Eng. Phys.*, 1998, **20**, 92.
31 Y. Liu, Z. Xu, W. Gao, Z. Cheng and C. Gao, *Adv. Mater.*, 2017, **29**, 1606794.
32 X. Bai, S. Liao, Y. Huang, J. Song, Z. Liu, M. Fang, C. Xu, Y. Cui and H. Wu, *Nano Lett.*, 2017, **17**, 1883.
33 J. Sun, Y. Li, Q. Peng, S. Hou, D. Zou, Y. Shang, Y. Li, P. Li, Q. Du, Z. Wang, Y. Xia, L. Xia, X. Li and A. Cao, *ACS Nano*, 2013, **7**, 10225.
34 M. Zhang, Y. Wang, L. Huang, Z. Xu, C. Li and G. Shi, *Adv. Mater.*, 2015, **27**, 6708.
35 S. Wang, J. Dong, Z. Li, Y. Xu, W. Tan, X. Zhao and Q. Zhang, *J. Appl. Polym. Sci.*, 2016, **133**, 43727.
36 R. Wang, J. Sun, L. Gao, C. Xu and J. Zhang, *Chem. Commun.*, 2011, **47**, 8650.

37 M. K. Shin, B. Lee, S. H. Kim, J. A. Lee, G. M. Spinks, S. Gambhir, G. G. Wallace, M. E. Kozlov, R. H. Baughman and S. J. Kim, *Nat. Commun.*, 2012, **3**, 650.
38 W. S. Hummers and R. E. Offeman, *J. Am. Chem. Soc.*, 1958, **80**, 1339.
39 Z. Xu and C. Gao, *Acc. Chem. Res.*, 2014, **47**, 1267.
40 J. Zhang, W. Feng, H. Zhang, Z. Wang, H. A. Calcaterra, B. Yeom, P. Hu and N. A. Kotov, *Nat. Commun.*, 2016, **7**, 10701.

Published on 01 August 2017. Downloaded by Zhejiang University on 22/08/2017 02:12:57.


This journal is © The Royal Society of Chemistry 2017